Thermodiffusion of polycyclic aromatic hydrocarbons in binary mixtures

Sara M. Hashmi, Sid Senthilnathan, and Abbas Firoozabadi

Citation: The Journal of Chemical Physics **145**, 184503 (2016); doi: 10.1063/1.4966191
View online: http://dx.doi.org/10.1063/1.4966191
View Table of Contents: http://aip.scitation.org/toc/jcp/145/18
Published by the American Institute of Physics

Thermodiffusion of polycyclic aromatic hydrocarbons in binary mixtures

Sara M. Hashmi,[a] Sid Senthilnathan, and Abbas Firoozabadi[b]
Department of Chemical and Environmental Engineering, Yale University, New Haven, Connecticut 06510, USA

(Received 15 July 2016; accepted 11 October 2016; published online 9 November 2016)

Thermodiffusion in liquid mixtures may explain some counter-intuitive but naturally occurring phenomena such as hydrocarbon reservoirs with heavier component(s) stratified on top of lighter ones. However, beyond benchmark systems, systematic measurements of thermodiffusion in binary organic mixtures are lacking. We use an optical beam deflection apparatus to simultaneously probe Fickian and thermal diffusion in binary solution mixtures of polycyclic aromatic hydrocarbons dissolved in alkanes, and measure both Fickian diffusion D and the Soret coefficient S_T, and then obtain the thermodiffusion coefficient D_T. In a series of nine binary mixtures, we vary both the size of the aromatic compound from two to four rings, as well as the length of the alkane chain from 6 to 16 carbons. To probe the effect of increasing ring size, we include a 6-ringed aromatic compound, coronene, and toluene as a solvent, due to the insolubility of coronene in alkanes. Our results suggest that Fickian diffusion increases with the inverse of solvent viscosity and also with decreasing molecular weight of the solute. While both of these trends match our intuition, the behavior of S_T and D_T is more complicated. We find that S_T and D_T increase with the solute molecular weight when the solvent is held fixed and that the impact of solute ring size is higher in shorter chain alkane solvents. *Published by AIP Publishing.* [http://dx.doi.org/10.1063/1.4966191]

INTRODUCTION

Diffusion refers to a mass transfer that can occur even in the absence of bulk motion. Primary diffusive fluxes occur down concentration gradients in binary mixtures, for instance to uniformly distribute molecules of solute in a solvent. Thermodiffusion refers to a secondary transport mechanism in which temperature gradients rather than concentration gradients cause mass transfer in binary or multicomponent mixtures. One rule of thumb suggests that the greater the difference between two molecules, the more they tend to separate when placed under an applied temperature gradient. However, there are many ways to measure the "similarity" or "difference" between molecules, including in terms of their molecular weight, shape, dielectric properties, inter-molecular potentials, solvent interactions, and other characteristics. Depending on which characteristic is chosen, the rule of thumb that "different molecules experience greater thermophoretic separation" may not always apply.

Thermodiffusion plays an important role in many small-scale biological phenomena and applications and on a very large scale may help to account for the observation of "upside-down" geological reservoirs, which are stable despite having a denser component lying on top of lighter ones.[1] Geological reservoirs contain complicated mixtures of oils, which can be branched and linear alkanes and alkenes, as well as aromatic compounds (Rx) from small ringed systems to larger resins and asphaltenes, which may contain alkane branches and a variety of functional groups in addition to an aromatic core. The aromatic nature of asphaltenes makes them more unstable than other components in largely aliphatic hydrocarbon reservoirs. While it is understood that the instability of asphaltenes has much to do with the contrast between their aromaticity and the aliphatic nature of many of the other components of petroleum fluids, complete thermodynamic descriptions of hydrocarbon reservoirs remain lacking. In order to better understand species distribution and the complex dynamics and thermodynamics in such reservoirs, a wide variety of mixtures must be studied. Binary solutions with one aliphatic component and one aromatic component are important mixtures to consider.

Investigations of thermodiffusion in mixtures of non-polar liquids have revealed some interesting features. Most binary systems studied to date are composed of two miscible liquids, such as the hexane-toluene system and binary mixtures of the three Fontainebleau benchmark compounds tetrahydronaphthalene, isobutylbenzene, and dodecane.[2–4,7] In binary mixtures of heptane with linear alkanes, molecular diffusion slows with an increasing molecular weight difference between the components.[6] On the other hand, thermal separation increases as heptane is mixed with alkanes of increasing chain length between 10 and 18 carbons.[6]

In some binary mixtures, differences in molecular weight can largely explain the Soret effect. For instance, the isotopic contribution to the Soret effect can be largely understood by considering differences in the molecular masses and moments of inertia in isotopic mixtures of similar polarity and aromaticity.[8,9] Binary mixtures of bromo-, chloro-, and fluoro-benzene were used to isolate the isotopic contribution

[a]Author to whom correspondence should be addressed. Electronic mail: sara.hashmi@yale.edu
[b]E-mail: abbas.firoozabadi@yale.edu

to the Soret effect and compare to theory.[9] Molecular mass and moment of inertia considerations have recently been used in molecular dynamics simulation to predict the thermodiffusion in mixtures of isotopic argon like atoms.[10]

The effect of molecular shape on binary thermodiffusion has been investigated using branched or linear alkanes, all containing seven carbons, mixed with either cyclic or aromatic ringed molecules benzene, cyclohexane, and xylene.[5] In these mixtures, the Soret coefficient (S_T) increases as a function of branching in the alkane component.[5] The effect of the changes in the ringed structure on thermal separation is less clear: of the three ringed compounds, benzene and xylene are aromatic, while cyclohexane is not. Xylene is further distinguished from benzene by the addition of two methyl groups. The C–H bonds of methyl groups and alkane solvents (Cx) alike have a non-zero dipole moment, while aromatic ring structures are often considered to have a net dipole moment of zero.[11] Quantum fluctuations of the dipole moment, which contribute to the Casimir effect, have recently been linked to the Soret effect.[12,13] Theoretical investigation suggests that the magnitude of the Casimir force is proportional to square of the Soret coefficient in binary mixtures.[13] One obvious next step in improving our understanding of the effect of aromaticity on thermally induced separation involves collecting data on a wider variety of aromatic compounds whose properties are varied in a systematic manner.

Studying larger aromatic compounds beyond single ringed-compounds will also improve our understanding of thermodiffusion phenomena in hydrocarbon reservoirs. It is clear from the molecular structure of the compounds in the present investigation that it is the difference in shape, and not simply the molecular weight difference, that will play the most important role in determining the thermodiffusion behavior of these binary mixtures. In particular, the fused ringed structure of the aromatic compounds under investigation makes them polycyclic aromatic hydrocarbon (PAH) compounds. Aromaticity, as in the single ringed molecule benzene, refers to the conjugation of C–C bonds and subsequent delocalization of electrons in p-orbitals both above and below the plane of the molecule. While unsubstituted aromatic molecules consist entirely of C and H and are still considered non-polar compounds, their electronic configuration sets them apart from aliphatic molecules also composed entirely of C and H atoms. While adding fused rings to a PAH compound gives the possibility for an increasingly large area of delocalized electrons, aromaticity may not increase in a linear manner with the number of rings. In PAH compounds with multiple fused rings, the degree of aromaticity, or electronic delocalization, can vary from ring to ring within a single molecule, and computations are needed to fully quantify aromaticity and electronic configurations.[14,15] To investigate the importance of ring size in the separation of PAH compounds from alkanes, we must expand the scope of study beyond liquid-liquid mixtures, as PAH compounds are solid at room temperature.

In this report, we present the first known measurements of thermodiffusion of polycyclic aromatic compounds dissolved in alkane solvents. By measuring three aromatic compounds, with two, three, and four fused aromatic rings, in each of three alkane solutions, hexane, decane, and hexadecane, we investigate simultaneously the effect of both chain length of the aliphatic compound and ring size of the aromatic compound. To further extrapolate the effect of increasing ring size on thermal separation, we also present measurements on four aromatic compounds, including one with six fused aromatic rings, each dissolved in toluene (tol). To the best of our knowledge, this type of picture has not been presented in the literature.

Using an Optical Beam Deflection (OBD) apparatus designed for the measurement of thermodiffusion in binary mixtures, we measure nine binary solution mixtures of aromatic compounds composed of 2–4 rings dissolved in alkane solvents. We compare our results to the literature data on benzene and methylated aromatic liquids mixed with alkanes. To investigate aromatic compounds with additional rings, we include the six-ringed coronene, which is insoluble in alkanes but soluble in toluene. As our intuition suggests, Fickian diffusion coefficient D decreases with the size of the component molecules and increasing solvent viscosity. However, the behavior of both the Soret coefficient S_T and the thermodiffusion coefficient D_T has a more complicated dependence on material parameters and are more strongly dependent on the size of the aromatic component than on the aliphatic solvent. Increasing the solute ring size increases both S_T and D_T when the alkane solvent is fixed. Shorter chain alkane solvents enhance the importance of the solute ring size, with the largest measurements of S_T and D_T found in the mixture of the largest aromatic compound, with four rings, dissolved in shortest alkane, hexane.

MATERIALS AND METHODS

Materials

In this study, we investigate three aromatic compounds dissolved in three different alkane solvents and four aromatic compounds dissolved in toluene. In addition to these 13 binary mixtures of aromatic compounds dissolved in alkane solvents and toluene, we also investigate mixtures of hexane-toluene, to validate our experimental setup. The aromatic compounds naphthalene, phenanthrene, pyrene, and coronene are obtained at 98%-99% purity from Acros Organics. The solvents are obtained at 99% purity from Alfa Aesar (decane, hexane, and toluene) or MP Biomedicals (hexadecane).

Table I introduces the compound names, molecular formulas, molecular weights, and the solvent viscosities. Data plots follow the marker style convention indicated in Fig. 1, which shows the molecular configuration of each compound and is labeled with the abbreviations used to indicate each aromatic compound (Rx), alkane solvent (Cx), and toluene (tol). The aromatic compounds are assigned colors: black for R2, red for R3, blue for R4, and orange for R6, while the solvents are assigned marker styles: diamonds for C16, stars for C10, squares for C6, and triangles for toluene. Note that coronene, R6, is insoluble in the alkanes.

Stock solutions of the aromatic compounds in each solvent are prepared in a nitrogen glove-box, to prevent the

TABLE I. Chemical names, molecular formulae, and molecular weights for each of the aromatic and alkane compounds in the present study. Table also gives μ the viscosity of the solvents in mPa s.

Aromatic compound	Molecular formula	Molecular weight (g/mol)	Solvent	Molecular formula	Molecular weight (g/mol)	Solvent viscosity (mPa s)
Naphthalene	$C_{10}H_8$	128.17	Hexane	C_6H_{14}	86.18	0.294
Phenanthrene	$C_{14}H_{10}$	178.23	Decane	$C_{10}H_{22}$	142.29	0.920
Pyrene	$C_{16}H_{10}$	202.25	Hexadecane	$C_{16}H_{34}$	226.44	3.040
Coronene	$C_{24}H_{12}$	300.36	Toluene	C_7H_8	92.14	0.590

uptake of water by the hygroscopic aromatic solid compounds, at a range of concentrations c, referring to the mass fraction of the aromatic compound. Unlike liquid-liquid binary mixtures, the solutions of aromatic compounds dissolved in alkane solvents have a limited range of accessible values of c due to solubility limitations. Table II gives the solubility limits c_s for each of the aromatic-alkane binary systems measured. The solubility of the compounds in the alkane solvents does not exceed 15% by mass. The smallest ringed compound, R2, has the highest solubility of the three aromatic materials in each of the solvents, ~12%–13%, while R3 and R4 solubility is closer to ~2%–3%. For each Rx-Cx mixture, measurements are taken using normalized concentrations c/c_s ranging from ~0.2–0.95. The hexane-toluene binary mixtures are prepared using 4 mass fractions of toluene ranging from $c \sim 0.27$ and 0.76.

Contrast factor measurements

We use an Anton Paar refractometer to measure the optical contrast factors $\mathrm{d}n/\mathrm{d}T$ and $\mathrm{d}n/\mathrm{d}c$, where n is the refractive index and T temperature. Between 6 and 15 measurements are taken on each sample, using a sample size between 100 and 200 μl. To measure $\mathrm{d}n/\mathrm{d}T$, we choose a fixed concentration and use the temperature range between 23 and 27 °C, with a 1 °C increment. We confirm that $\mathrm{d}n/\mathrm{d}T$ is independent of concentration by measuring the binary mixture R2-C16 at two different concentrations, $c = 0.06$ and $c = 0.12$. Despite a factor of 2 difference in c, the resultant difference in $\mathrm{d}n/\mathrm{d}T$ is less than 1.8%. To measure $\mathrm{d}n/\mathrm{d}c$, we obtain between 6 and 9 data points for each mixture along with n of the pure solvents. There is a slight dependence on T for measurements of $\mathrm{d}n/\mathrm{d}c$: for the R2-C16 binary mixture, $\mathrm{d}n/\mathrm{d}c = 0.1387$ at $T = 20$ °C and $\mathrm{d}n/\mathrm{d}c = 0.1429$ at $T = 23$ °C, an increase of 3% over the 3 °C difference. Hence we fix $T = 25.5$ °C for measurements of $\mathrm{d}n/\mathrm{d}c$, to match the conditions in the thermodiffusion measurements.

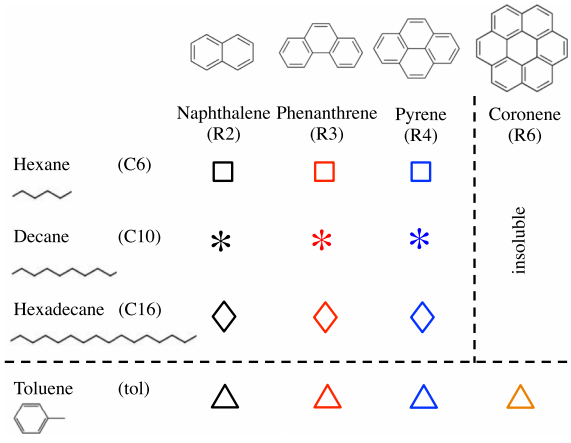

FIG. 1. Molecules and mixtures measured: we investigate 9 binary systems of aromatic molecules dissolved in alkane solvents and 4 binary systems of aromatic molecules dissolved in toluene. The molecular formulas are given for each component, with the abbreviations used to refer to them in parentheses. The symbols shown in Figure 1 are used consistently in subsequent figures to denote each mixture. By investigating nine binary solutions of aromatics in alkanes, we investigate both effects of increasing chain length and increasing ring size on thermal and Fickian diffusion.

The refractometer operates at the sodium D-line, 589 nm, while the thermodiffusion experiment uses a laser at 632 nm (red). We assess the effect of the difference in wavelength on contrast factor measurements by using hexane-toluene mixtures. At 589 nm, we measure $\mathrm{d}n/\mathrm{d}c = 0.117$, within ~2% of the measured value $\mathrm{d}n/\mathrm{d}c = 0.120$ at 632 nm.[2] As a point of comparison, contrast factors for ethanol-water systems from different sources, even obtained at the same wavelength, can vary up to 3%.[16]

Figure 2 shows the compiled results for $\mathrm{d}n/\mathrm{d}T$ (a) and $\mathrm{d}n/\mathrm{d}c$ (b). The number of carbons in the alkane solvent most strongly determines the behavior of $\mathrm{d}n/\mathrm{d}T$, as shown in Fig. 2(a). There is a 20% increase in $\mathrm{d}n/\mathrm{d}T$ from the C6 binaries to the C16 binaries, from $\sim -5.1 \times 10^{-4}$ K^{-1} to $\sim -4.2 \times 10^{-4}$ K^{-1}. The dependence of $\mathrm{d}n/\mathrm{d}T$ on the number of aromatic rings is slight: for C10 and C16, $\mathrm{d}n/\mathrm{d}T$ varies only ~2% when considering the three aromatic compounds. The variation is slightly more for C6 but still less than 5%. As a point of comparison, $\mathrm{d}n/\mathrm{d}T = -5.5 \times 10^{-4}$ K^{-1} for hexane-toluene mixtures and is treated as concentration-independent over the entire range from 0.05 to 0.95 mass fraction of toluene in hexane.[2] The number of rings in the aromatic compounds most strongly determines the behavior of $\mathrm{d}n/\mathrm{d}c$, as shown in Fig. 2(b). There is a 50% increase in $\mathrm{d}n/\mathrm{d}c$ from the R2 binaries to the R4 binaries. The dependence of $\mathrm{d}n/\mathrm{d}c$ on the length of the alkane solvent chain is slight: for R3 and R4, $\mathrm{d}n/\mathrm{d}c$ varies only 3% or less when considering the three alkane solvents. The variation is slightly more for R2, at ~7%.

TABLE II. Solubility limit c_s (by mass %) for each of the nine binaries.

	R2	R3	R4
C6	12.5	3.0	2.0
C10	13.5	3.1	3.0
C16	12.0	3.0	2.3

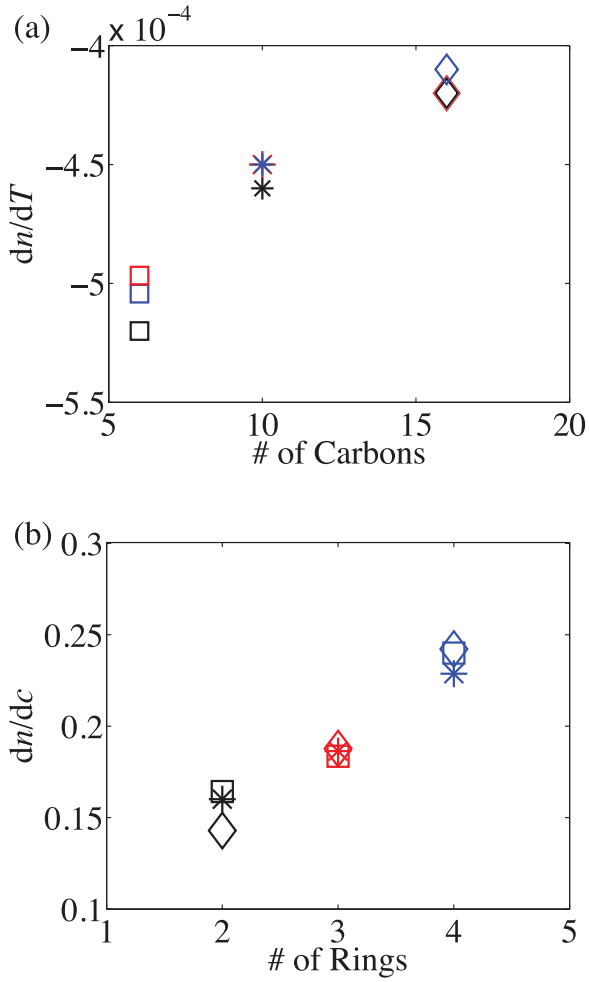

FIG. 2. Compilation of contrast factor measurements for the nine binary mixtures of aromatic compounds in alkane solvents: (a) shows dn/dT as a function of the length of the solvent chain, while (b) shows dn/dc as a function of the number of rings in the aromatic compound. In (a), each data set indicates a different aromatic compound as listed in the legend, while in (b), each data set indicates a different alkane solvent as listed in the legend.

Optical cell

In the Optical Beam Deflection (OBD) technique, a mixture is enclosed in a quartz glass ring sandwiched between two parallel, horizontal, temperature-controlled copper plates. The quartz glass rings are set in grooves milled into the copper plates, with O-rings (McMaster-Carr, Viton) sealing the copper-glass connection. Precision spacers (±10 μm, Delrin) sit inside the corners of the assembled cell to ensure the plates are parallel. Cylindrical quartz glass (Technical Glass Products) with an inner diameter 60 mm is cut into rings and the surfaces are polished to a tolerance of ±10 μm. For the validation runs using hexane-toluene mixtures, h = 7.62 mm, while for the aromatic mixtures, h = 4.56 mm.

The liquid sample is input into the cell via a syringe (Hamilton Gastight) connected to the stainless steel capillary inlet. The sample is flushed into the cell and through the stainless steel capillary outlet upon filling. During experimental runs, the stainless steel capillary outlet is closed with a Teflon stopper to prevent evaporation. To swap samples of the same binary mixture at different concentrations, several cell volumes of the new sample are flushed through the cell to ensure a complete exchange from the initial concentration to the final concentration. Measurements of the refractive index n of the collected samples confirm the concentrations. To change the binary mixture entirely from one binary to another, the entire cell is disassembled and cleaned. Separate syringes are dedicated to each aromatic compound to protect against cross-contamination between the mixtures.

The optical measurement system is composed of a laser light source, a telescope to reduce the spot size of the laser, the measurement cell, and a linear detector, as shown in Fig. 3(a). A horizontal laser beam (632 nm) first passes through a neutral density (ND) filter (Thorlabs). The telescope, comprised of lenses R1 and R2 with focal lengths of 300 and 100 mm, respectively, reduces the spot-size of the optical beam by a factor of 3. After passing through a pinhole to limit any stray light, the optical beam enters the cell, centered in the middle of the vertical dimension, and its vertical position is read by a linear detector (UDT) on the other side. Figure 3(b) provides a schematic of the cell itself. In Figs. 3(a) and 3(b), the dimensions labeled l, l_w, l_d, and h are those that determine the magnitude of the signal read at the face of the detector. In our experimental setup, l = 60 mm and l_w = 2 mm as determined by the geometry of the copper plate assembly. Both h and l_d can be varied by either changing the quartz glass ring or the position of the detector. For the validation runs, these parameters are h = 7.62 mm and l_d = 279 mm, while for the measurement runs, they are h = 4.56 mm and l_d = 356 mm.

Temperature control

Temperature control on the copper plates is accomplished by a set of thermofoil heaters (Minco) adhered to the outer surfaces of each plate. Currents through the top and bottom plate heaters are driven by two independent variable

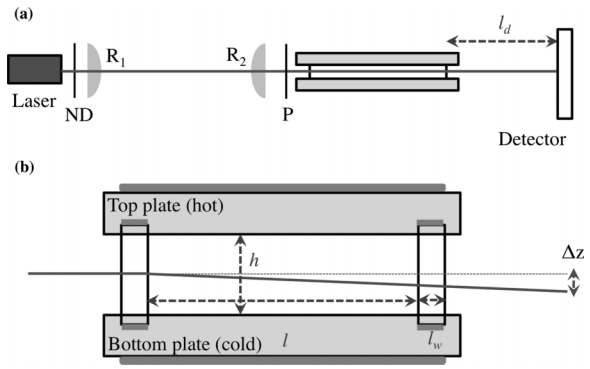

FIG. 3. Schematic and pictures of the setup. (a) shows the optical path, from the laser, through a neutral density (ND) filter, two lenses (R1 and R2), a pinhole (P), and the cell to the detector. The schematic in (b) shows the cell itself: two copper plates sandwiching O-rings and a quartz glass ring to form a sample chamber of height h and length l. The optical beam is shown as a solid line as it passes through the sample and to the detector where the deflection is measured. The labels l, l_w (window length, in (a)) and l_d (length to the detector, in (b)) correspond to those used in Equation (4). The label Δz refers to the displacement of the laser signal in the z direction on the detector. The drawings are not to scale.

voltage power supplies. Temperature on the plates is read via thermistors (Measurement Specialties, 46 037) inserted into tapholes in each plate. The resistance of the NIST-calibrated thermistors is read via custom-built electronics, consisting of one Wheatstone bridge and one signal amplifier (Tacuna) for each thermistor, with the voltage output of the amplifiers sent to a data acquisition system (NI cDAQ). A closed-loop proportional-integral-derivative (PID) system coded in LabView compares the measured temperatures to the set points. The output PID signal is sent through the data acquisition interface, the voltage outputs of two 30 V power supplies to the heaters accordingly. The closed-loop system runs at approximately 1 Hz. Isolating the cell from ambient air flows is a key to obtaining the most stable temperature control on the plates. Additional thermostatting is only required if the ambient temperature rises above approximately 22 °C. The control loop maintains temperature on the copper plates within $< \pm 0.5$ mK of the desired set point.

Experimental procedure

Each experimental run is composed of two parts: a step where the temperature gradient between the plates is turned off and one where it is turned on. The steps are of equal duration and several times longer than the characteristic diffusion time $\tau_D = h^2/\pi^2 D$. Both top and bottom plate temperatures are controlled throughout. Typical measurement step times range from 2 h for C6 binary mixtures to 6 h for C16 binary mixtures. Two or three concentrations are measured for each binary mixture. We vary the temperature step size ΔT from 0.5 to 2 °C, using $\langle T \rangle = 25.5$ °C, to confirm that the thermodiffusion constants are independent of applied temperature gradient. Error bars on the measured thermodiffusion constants represent run-to-run variations based on 5–15 runs per mixture.

Once equilibrium is reached in the absence of a temperature gradient, the measurement begins with the application of a temperature gradient. A typical trace of the beam position z is shown in Fig. 4, for $c = 0.05$ of the R4-tol binary mixture. The trace in Fig. 4(a) shows the end of the step where $\Delta T = 0$ °C, and the temperature gradient is turned on to $\Delta T = 1$ °C at $t = 0$. First, due to the change in temperature and the thermal diffusivity α of the mixture, the index of refraction n of the mixture immediately changes, causing the optical beam to bend in the vertical direction. The overshoot in the position z is due to an overshoot in reaching the set point temperature on the upper plate, which lasts approximately 30 s. The initial movement of more than 3 mm can be seen at $t = 0$.

As Fickian and thermal diffusive behavior begins to manifest, the mixture separates. As the concentration gradient evolves in the vertical direction, so too does the index of refraction, causing bending of the optical beam and movement in the vertical z-direction. This can be seen more clearly in Fig. 4(b), where the data are shown in gray: diffusion causes a gradual bending of the beam starting at approximately t ~300 s. The instantaneous fluctuations in the beam position are <2 μm, arising from instantaneous fluctuations in ΔT of ~0.2 mK, and are comparable to the root-mean-squared error of the fitted curve shown in black. The duration of the measurement is 2.5 h, which in this case corresponds to ~$6\tau_D$.

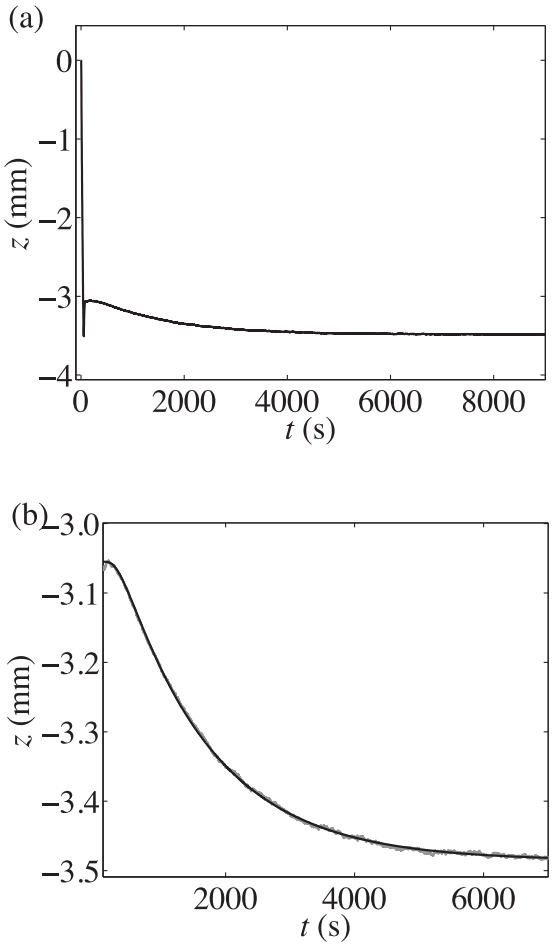

FIG. 4. Example of a typical beam deflection measurement, using $c = 0.05$ for the R4-tol mixture. (a) shows the entire trace, while (b) shows an enlargement of the signal motion due to the combination of Fickian and thermal diffusion, with the fit to Eqs. (1)-(4) overlaid in black.

DATA ANALYSIS AND MATHEMATICAL FRAMEWORK

The bending of the optical beam as a function of time is used to extract both the Fickian (D) and Soret coefficient (S_T) of the mixture according to four transport and optical equations, given below. The heat equation (Eq. (1)) determines the establishment of the temperature gradient through a liquid with thermal diffusivity α. The extended diffusion equation (Eq. (2)) gives changes in concentration c as a result of both Fickian and thermal diffusion, provided that convection can be neglected. A complete derivative (Eq. (3)) gives the gradient of refractive index n in the vertical direction z due to changes in both temperature and concentration. Snell's law for optical refraction (Eq. (4)) denotes the bending of the beam in the vertical direction given the geometry of the cell as labeled in Fig. 3(b), and as a result of changes in the refractive index gradient. Snell's law applied to the thermodiffusion cell has been derived in the literature.[2,17] For binary systems, these

four equations are given below,

$$\frac{\partial T}{\partial t} = \alpha \nabla^2 T, \tag{1}$$

$$\frac{\partial c}{\partial t} = D\nabla^2 c + D_T \nabla^2 T, \tag{2}$$

$$\frac{dn}{dz} = \left(\frac{\partial n}{\partial T}\right)\frac{dT}{dz} + \left(\frac{\partial n}{\partial c}\right)\frac{dc}{dz}, \tag{3}$$

$$\delta z = L\frac{dn}{dz}\left(\frac{L}{2n} + \frac{l_w}{n_w} + \frac{l_d}{n_{air}}\right). \tag{4}$$

The above set of equations is used to extract D and D_T as fitting parameters from measurements of the beam deflection δz.[18] Alternatively, D and S_T can be reported, where

$$S_T = \frac{D_T c(1-c)}{D} \tag{5}$$

is defined for binary mixtures only.[2] For optical beam measurements, D and S_T are the parameters of choice, as they are decoupled from each other in predicting the measured behavior and provide two independent parameter choices. D is determined from the bending of the beam at moderate time scales, while S_T is determined by the steady-state deflection of the optical beam. The contrast factors dn/dc and dn/dT used in Eq. (3) must be measured independently, as discussed above.

The solution to the above system of equations contains two time scales: a fast time scale denoting thermal conduction through the liquid sample, $\tau_c = h^2/\pi^2\alpha$, and a slow time scale for diffusive mass transfer, $\tau_D = h^2/\pi^2 D$. For instance, in hexane-toluene mixtures, using $h = 7.62$ mm, $\tau_c \sim 60$ s while τ_D ranges from 1660 to 2360 s.[2,17] For C16 mixtures, using $h = 4.56$ mm, τ_c decreases to ~20 s, while τ_D increases to ~3500 s. Due to the separation of time scales, $\tau_D \gg \tau_c$, the processes of thermal conduction and thermal diffusion are decoupled: any short-lived fluctuations in temperature on the two plates manifest as short-lived fluctuations in the beam position only. These fluctuations can be predicted in a straightforward way by integrating Eq. (1) using the time-dependent boundary conditions given by the time-dependent temperature on each plate.[16,19] However, given the low magnitude of fluctuations in our measurements, we use fixed boundary conditions in solving Eqs. (1)-(4). The overlaid fit to the data in Figure 4(b) corresponds very closely to the measurement.

Instrument verification

We verify the OBD setup using a binary liquid mixture of toluene and hexane, comparing to the standard calibration curve presented by Zhang *et al.*[2] To measure this binary, we use a cell with $h = 7.562$ mm and $l_d = 279$ mm, four different concentrations, and several values of ΔT.

We investigate binary mixtures of hexane and toluene with our thermodiffusion instrumentation, use the solution to Equations (1)-(4) to extract measurements of D and S_T, and compare them to the literature standard.[2] Experiments are run for 2-3 h each, using applied temperature gradients between 1.3 and 3 °C. The length of the experiments corresponds to at least $\sim 4\tau_D$ for all mixtures investigated. We use 4 different concentrations, all listed in terms of mass fraction of toluene: 0.2685, 0.4788, 0.517, and 0.7563. Of these, 0.517 was measured by Zhang *et al.*[2] Our concentrations of 0.2685 and 0.7563 are within 2.3% and 0.4% of the concentrations 0.2627 and 0.7623 measured by Zhang *et al.*, respectively.[2] Figs. 5(a) and 5(b) show our validation results overlaid on top of the original data from Zhang *et al.*, for fitted values of D in (a) and S_T in (b). The solid black lines in each plot indicate the polynomial fits of D and S_T determined by Zhang *et al.* The polynomial for D is second order in both c and T, while the polynomial for S_T is third order in c and second order in T. In Fig. 5, the data and fits from Zhang *et al.* are shown for an average temperature $\langle T \rangle = 25$ °C. Table III shows the results of our instrument verification, with the average value of D and S_T for each value of c investigated, as well as the % deviation from the standard calibration curves provided by Zhang *et al.*

All measured values of both D and S_T are within 2.7% or less from the values obtained by using the polynomials $D(c,T)$ and $S_T(c,T)$ provided by Zhang *et al.*[2] Furthermore, the results at $c = 0.517$ are obtained from four independent runs: the average measurement $D = 277.5 \pm 5.2 \times 10^{-5}$ mm^2/s, a spread of 1.9% for the four data sets. The same runs provide an aggregate measurement $S_T = 485.75 \pm 3.4 \times 10^{-5}$ K^{-1}, giving a spread of 0.7% for the four data sets. In general, the fits for

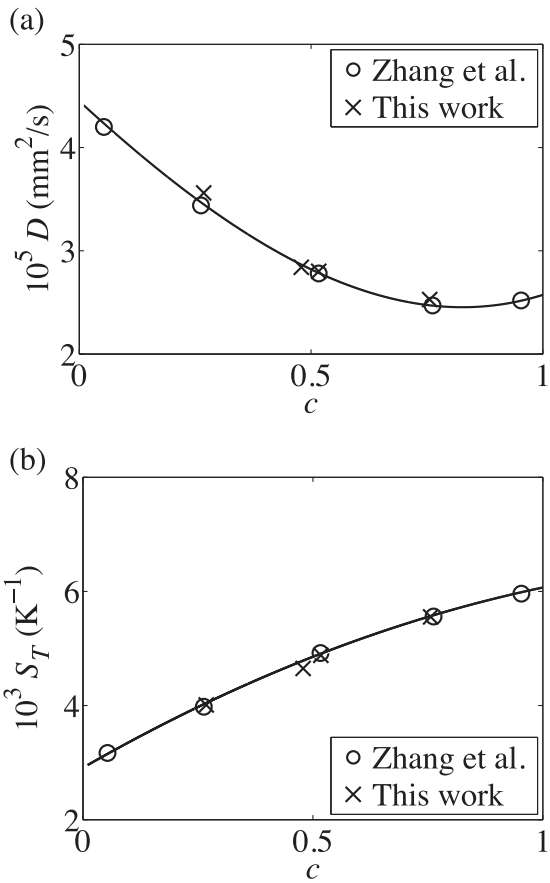

FIG. 5. Validation results are plotted by ×'s overlaid on the values from Zhang *et al.*, denoting with points, and the solid lines in each plot indicate the polynomial fits determined by Zhang *et al.*[2]

TABLE III. Validation results for hexane-toluene mixtures. Tabulated values include the concentration c in mass fraction of toluene, the fitted values of both D and S_T, along with the % error compared to the literature values.

c	$10^5 D$ (mm^2 s^{-1})	% from standard	$10^5 S_T$ (K^{-1})	% from standard
0.2685	354	1.2	403	0.1
0.4788	284	−2.7	464	−2.1
0.5170	278	−1.2	486	−1.6
0.7563	253	1.8	555	0.2

S_T are slightly better in comparison to the literature standards than the fits for D: for D, the % difference from Zhang's calibration curve ranges from 1.2% to 2.7%, while for the S_T values, the % difference from Zhang's calibration curve ranges from 0.1% to 2.1%. The fact that S_T is in general measured to greater precision than D is also well known in the literature.[16,19] Furthermore, all values fall within the range of less than 1% to less than 3% variation indicated by Zhang *et al.* in their own measurements.[2]

RESULTS AND DISCUSSION

This report documents the thermodiffusion measurements of nine binary mixtures of aromatic compounds dissolved in alkanes, as well as four binary mixtures of aromatics dissolved in toluene.

Fickian diffusion *D*

Figure 6(a) shows D as a function of concentration for the nine aromatic-alkane mixtures, with many of the error bars smaller than the size of the data points. Given the range in values of c_s for the solutions, we plot D as a function of the normalized concentration c/c_s. We first discuss the behavior of D, shown in Fig. 6(a). In general, the results are grouped mainly by solvent: C16 binaries (diamonds) have the lowest value of D, while C10 binaries (stars) all have an intermediate value of D, and the C6 binaries (squares) exhibit the largest D. Keeping each aromatic compound fixed, D increases by roughly a factor of 2.5 as the solvent changes from C16 to C10, and again by a factor of 2-3 from C10 to C6. Decreasing the alkane chain length results in an increase of D for all three aromatic solutes. This result matches our intuition that a given solute molecule will diffuse more rapidly in a solvent whose molecules are smaller than in a solvent whose molecular size is larger. Furthermore, the factors of ~2.5 are fairly close to the viscosity ratios $\mu_{C16} : \mu_{C10} = 3.3$ and $\mu_{C10} : \mu_{C6} = 3.1$, respectively. Again this qualitative agreement matches our intuition from Stokes drag on a sphere, which varies directly with the solvent viscosity. Within the three sets of C16 and C10 binaries, the larger aromatic ring binaries diffuse more slowly than the smaller ones, with R4 (blue) having the smallest D, R3 (red) an intermediate value, and R2 (black) the largest value of D. The same qualitative dependence on the aromatic ring system is seen in the C6 binaries, with the R2-C6 binary having a larger value of D than the R4-C6 binary, but the difference between the aromatic compounds is much less in C6 than in either C10 or C16. None of the nine aromatic-alkane solutions exhibit any significant dependence of D on c/c_s.

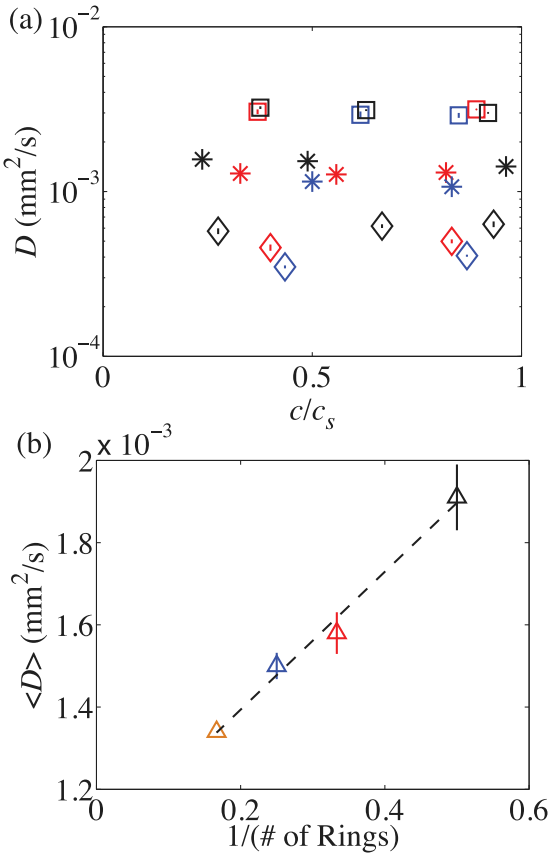

FIG. 6. (a) D as a function of c/c_s for the nine binary solutions of aromatics dissolved in alkanes. (b) shows $\langle D \rangle$ as an inverse function of the number of rings in the aromatic solute compound, for the four aromatic compounds dissolved in toluene. The dashed line in (b) indicates a linear fit to the data. The color of the data points reflects the aromatic component, while the marker style indicates the alkane solvent: black indicates R2, red indicates R3, and blue indicates R4, while diamonds indicate C16, stars C10, and squares C6. In (b), triangles indicate toluene, while orange indicates R6. Some error bars are smaller than the data point size.

The impact of ring size can be seen more clearly when extended the aromatic compounds to R6. However, due to the insolubility of R6 in alkane solvents, we use toluene as the solvent for all four aromatic compounds, allowing for an assessment of the importance of ring size while keeping the solvent constant. Figure 6(b) shows $\langle D \rangle$ for the four binary mixtures of aromatic compounds dissolved in toluene. Given the relatively weak concentration dependence of D, $\langle\rangle$ denotes averages over the measured range of c. We find that $\langle D \rangle$ increases linearly with the inverse of the number of rings in the aromatic compound, as seen in Figure 6(b). The dashed line indicates a linear fit to the data, with a slope of 0.0017 mm^2/s.

Given that the number of rings in each compound may be considered a proxy for molecular size, the linear behavior seen in Figure 6(b) suggests that Brownian motion may explain the measured Fickian diffusion constant D. To investigate this possibility, we plot $\langle D \rangle$ as a function of $1/\mu$,

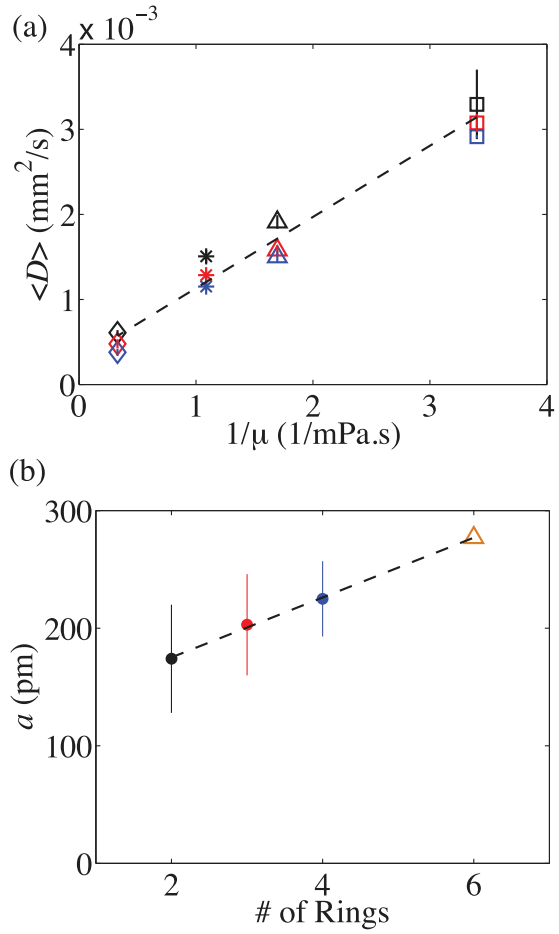

FIG. 7. (a) shows $\langle D \rangle$ as a function of $1/\mu$, the viscosity of the solvent for each mixture. The dashed line indicates a linear fit to the data. The color of the data points reflects the aromatic component, while the marker style indicates the alkane solvent: black indicates R2, red indicates R3, and blue indicates R4. In (a), diamonds indicate C16, stars C10, and squares C6. Some error bars are smaller than the data point size. (b) shows estimates of the molecular size a based on the Stokes-Einstein relation as a function of the number of rings in the aromatic compound, and the dashed line is a linear fit to the data. The points indicate averaged estimate based on all four solvents for R2 (black), R3 (red), and R4 (blue), while the orange triangle indicates the estimate for R6 based on the R6-toluene solution measurement.

the solvent viscosity. Indeed, as shown in Figure 7(a), D increases linearly with $1/\mu$. The dashed line indicates a fit to the data: $\langle D \rangle = m/(\mu) + b$, where $m = 8.3 \times 10^{-4}$ mm^2 mPa and $b = 2.9 \times 10^{-4}$ mm^2/s. This result matches our intuition from Stokes law, where Brownian diffusion scales as $1/\mu$. In binary liquid-liquid mixtures, the dependence of D on μ may require more complicated correlations, and Brownian motion does not fully capture the properties of one liquid diffusing within another.[3] However, because the binary mixtures under consideration here are solutes dissolved in solvents, the viscosity of the solvent dominates the diffusive behavior of the solute. The error bars in Figure 7(a) are less than 13% and indicate the range in D given the concentrations measured. The values of $\langle D \rangle$ are tabulated in Table IV.

Given that the mixtures under consideration are solutes dissolved in solvents, combined with the observation that D increases linearly with $1/\mu$, seen in Figure 7(a), we estimate the molecular size of the solute, a, using the Stokes-Einstein

TABLE IV. Measurements of the concentration-averaged values $\langle D \rangle$ for the twelve binary solutions of aromatic compounds dissolved in alkanes and toluene, as plotted in Figure 7(a). All values are listed in 10^5 mm^2 s^{-1}.

	R2	R3	R4
C6	329 ± 41	308 ± 11	291 ± 1.8
C10	151 ± 7.7	129 ± 5.5	115 ± 4.8
C16	61 ± 3.0	48 ± 5.5	38 ± 4.2
Toluene	191 ± 8.0	158 ± 5.7	150 ± 6.8

relation

$$D = \frac{k_B T}{6\pi\mu a}, \tag{6}$$

where k_B is the Boltzmann constant. While this relation is most often used to describe nanoparticle diffusion in suspension, here we use it to estimate the molecular size of the solute, with the assumption of a spherically shaped molecule. Using the measurements of $\langle D \rangle$, we obtain estimates of a from each of the 13 binary solutions: four solutions each with R2, R3, and R4 and one solution with R6. We average to find values of $a = 174 \pm 46$ pm for R2, 203 ± 43 pm for R3, and 225 ± 32 pm for R4. Even though these estimates are obtained using measurements in four distinct solvents for the aromatic compounds R2, R3, and R4, the spread in the estimates of a is at most 26% for each compound. For R6, using our measurement in toluene only, we find $a = 277$ pm. The molecular size estimates a are shown in Figure 7(b) as a function of the number of rings in each compound. The data points for R2, R3, and R4 represent averages over the four different solvents, while the estimate for R6 is shown with a triangle, to indicate the toluene solution. The dashed line represents a linear fit to the data, with a slope of 25 pm. As a point of comparison, crystallographic investigations of benzene reveal six identical C–C bonds all with length 139 pm.[20,21]

Soret coefficient S_T

The behavior of S_T, related to steady-state separation of the two components, is more nuanced than the behavior of Fickian diffusion D. By comparing Figures 6(a) and 8(a), we find that the measurements of S_T as a function of c/c_s in Figure 8(a) are not so neatly ordered by solvent. However, it seems that the solute may play a more important role: the three R2 binaries (black) exhibit lower S_T than the three R3 binaries (red). Two of the three R3 binaries in turn exhibit lower S_T than the three R4 binaries (blue). Interestingly, as we compare each set of aromatic binaries, the dependence on alkane solvent changes. For instance, with the R2 binaries, there is greater concentration separation in C10 than in C16 and even a slightly higher S_T for the R2-C6 binary than in the R2-C10 binary. But with the R3 binaries, there is greater thermal separation of the solutes in C16 than in C10.

Figure 8(b) shows the concentration averaged value $\langle S_T \rangle$ as a function of a the values for which are shown in Figure 7(b). Increasing the ring size to R6 has a pronounced impact on the

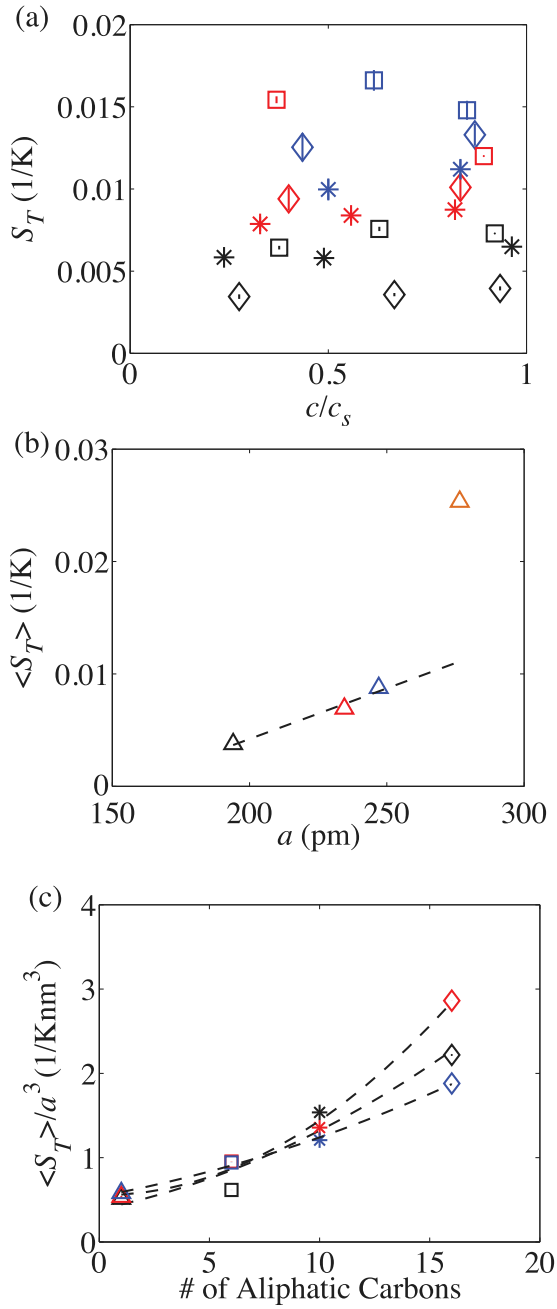

FIG. 8. (a) S_T as a function of c/c_s for the nine binary solutions of aromatics dissolved in alkanes. (b) shows $\langle S_T \rangle$ as a function of a for the four aromatic compounds dissolved in toluene. The dashed line in (b) indicates a linear fit to the data. (c) shows $\langle S_T \rangle / a^3$ as a function of the number of aliphatic carbons in each solvent. The dashed lines in (c) indicate quadratic fits to the data, with one fit per solute molecule R2, R3, and R4.

behavior of $\langle S_T \rangle$. The dashed line provides a linear fit to the data for R2, R3, and R4, with slope 9.9×10^{-4} mm^2/pm s. The measurement for R6 falls above the linear extrapolation for $\langle S_T \rangle$ based on molecular size.

Next we aim to rescale the concentration-averaged values $\langle S_T \rangle$ to collapse the data from Figure 8(a) onto a single curve. The trends in Figures 8(a) and 8(b) show that S_T increases with both the number of rings in the solute compound and the molecular size estimated from measurements of D. With solute size seeming to determine the magnitude of S_T, we normalize by a^3 the estimated volume of the solute molecules.

TABLE V. Measurements of the concentration-averaged values $\langle S_T \rangle$ for the twelve binary solutions of aromatic compounds dissolved in alkanes and toluene. All values are listed in 10^4 K^{-1}.

	R2	R3	R4
C6	71 ± 5.9	135 ± 15	157 ± 13
C10	60 ± 3.9	86 ± 3.8	106 ± 8.7
C16	37 ± 2.6	98 ± 4.9	129 ± 5.4
tol	38 ± 2.2	69 ± 2.7	88 ± 3.6

Furthermore, with recent suggestions that dipole moments play an important role in determining the Soret effect,[12,13] we plot $\langle S_T \rangle / a^3$ as a function of the number of aliphatic carbons in each solvent. The alkane solvents contain entirely aliphatic carbons, while toluene consists of an aromatic benzene ring with a single methyl group, and thus has a single aliphatic carbon. The resulting plot is shown in Figure 8(c), where the dashed lines represent quadratic fits to $\langle S_T \rangle / a^3$ as a function of the number of aliphatic carbons in the solvent. The collapse of S_T by a^3 may result from the free rotation of solute molecules in three dimensions as they both diffuse and migrate through the applied temperature gradient. The rescaling collapses the data best in solvents with fewer aliphatic carbons. Note that $\langle S_T \rangle / a^3$ for both R3-C6 (red square) and R4-C6 (blue square) mixtures lie nearly on top of each other. The values of $\langle S_T \rangle$ in Figure 8(c) are tabulated in Table V.

Thermodiffusion D_T

Given our measurements of the nine binary aromatic-alkane mixtures, we look into the literature for data comparisons. One of the barriers to developing more complete theories for thermodiffusive phenomena is the lack of data in the literature. There are several investigations of aromatics in alkanes, but none which systematically increase the ring size of the aromatic compound.[3,4,22–25] Other investigations look at alkane mixtures only or may vary alkane branching instead of chain length.[5,6]

In four of these papers, S_T for systems of benzene (R1) and heptane (C7) increases by a factor of 4 with increasing concentration, as measured by a variety of methods and with good agreement, as shown in Fig. 9(a).[22–25] S_T increases as a function of c, and, lacking a predictive theory, the line indicates a spline fit to the data. In two other papers, methylnaphthalene, mR2, is mixed with a series of alkanes to investigate the dependence of $D_T = S_T \times D$ on both concentration of the aromatic component and the alkane chain length, and the data are compiled in Fig. 9(b).[3,4] As the chain length of the alkane in an aromatic-alkane mixture increases, when the aromatic component is methylnaphthalene, the concentration-dependent behavior of D_T changes.[3,4] As shown in Fig. 9(a), when the alkane chain is short, as with C5 pentane, D_T decreases with c, by almost a factor of 2 from $c = 0.25$ to $c = 0.75$. The dashed line indicates a linear fit to the mR2-C5 mixture, with a slope of -32×10^{-6} mm^2/sK. As the chain length increases to 16, with hexadecane, however, the concentration dependence nearly vanishes.The dashed

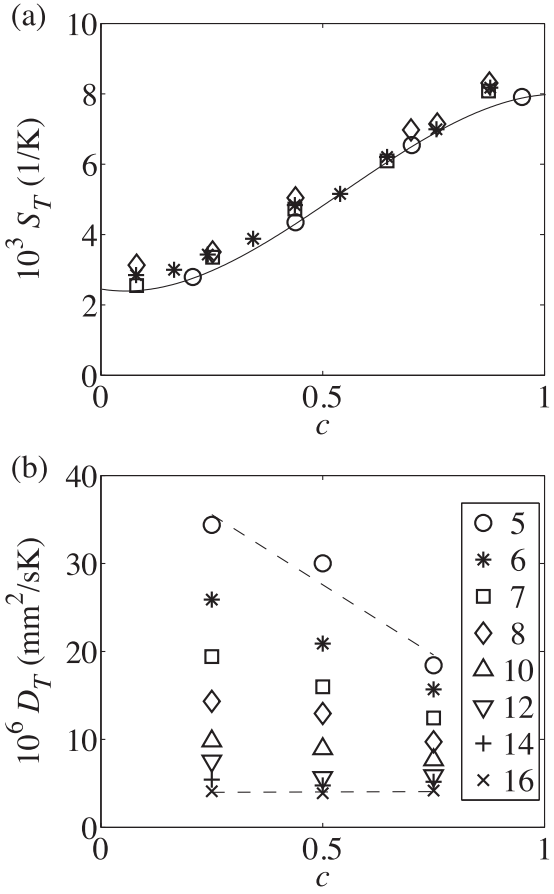

FIG. 9. The literature data showing the thermal separation of aromatics in alkanes: (a) shows S_T for benzene (R1) in heptane (C7) as a function of c, from a variety of sources as indicated in the text.[22–25] The line provides a spline fit to the data. (b) shows D_T as a function of c for methylnaphthalene (mR2) in a variety of alkane solvents, where the number of carbons is given in the legend.[3,4] The dashed lines indicate linear fits for mR2 in pentane (5) and in hexadecane (16). In both plots, c refers to the concentration of the aromatic component.

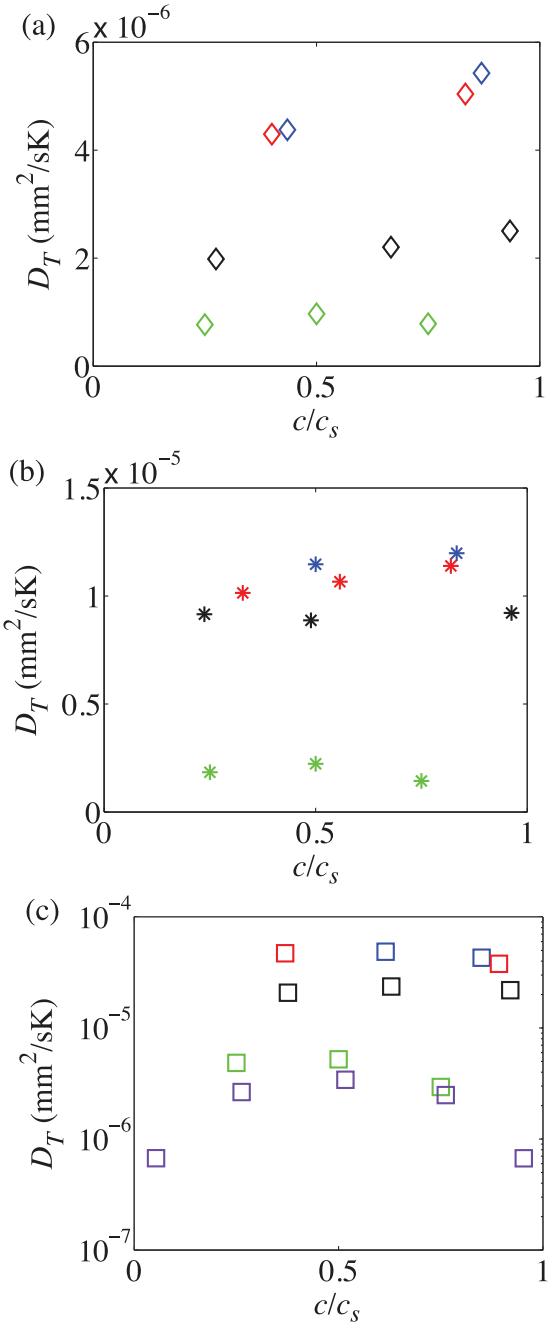

FIG. 10. D_T as a function of c/c_s for aromatic mixtures, with hexadecane binaries in (a), decane binaries in (b), and hexane binaries in (c). Data are shown with the same color and marker style convention as in Figure 6: black indicates R2, red indicates R3, and blue indicates R4. The literature data are overlaid on top of our data, with binaries of toluene (mR1) and C6 shown in purple squares in (c), and binaries of methylnaphthalene (mR2) shown in green in (a), (b), and (c).[2–4]

line indicates a linear fit to the mR2-C16 mixture, with slope 0 mm^2/sK.

Figure 10 indicates where our measurements fall in light of those in the literature. The binary systems we have investigated are new additions to the catalog of binary data but can be compared in a qualitative way to other measurements. Figure 10 is divided into constituent plots based on the alkane solvent used: C16 binaries are shown in (a), C10 binaries in (b), and C6 binaries in (c). As in our measured values of D and S_T, D_T does not exhibit significant concentration dependence. The concentration dependence of D_T is plotted for four mixtures for both C16 and C10: R2, R3, and R4, from our study, in addition to mR2, methylnaphthalene, from the literature.[3,4] In Figure 10, we plot our own data for R2, R3, and R4, comparing to data for mR2 and also mR1, toluene.[2–4] We plot all results against the normalized c/c_s, and note that for mR1 and mR2, which are liquids, $c_s = 1$ in the alkane solvents.

Investigation of the comparisons in Figure 10 may lend some insight into the effect of aromaticity and electronic configurations on thermodiffusion. In particular, the upper limit on the y-axis increases from (a) to (b) to (c). In general, an increasing ring size of the aromatic component leads to an increase in D_T. While the difference between aromatic behaviors is within a factor of about 4 or 5 in both C16 and C10, the difference between mR1 and mR2 compared to the non-methylated R2, R3, and R4 is more than a factor of 10 in C6; hence D_T is shown on a log scale in Figure 10(c). This observation may suggest that shorter chain alkanes can enhance the importance of ring size and aromaticity in determining thermodiffusive behavior.

CONCLUSIONS

We present measurements of aromatic compounds dissolved in alkane solvents and toluene. By increasing both aromatic ring size from two to four rings and the alkane chain length from 6 to 16 carbons, we observe the importance of molecular size and solvent viscosity in determining thermal and Fickian diffusion dynamics. By measuring polycyclic aromatic hydrocarbon compounds dissolved in solvents, we find that the Fickian diffusion can be explained in terms of Brownian motion of the solute molecules in the background solvent: a result not found in liquid-liquid systems. Using toluene as an additional solvent allows us to investigate the behavior of larger aromatic compounds with six fused aromatic rings. Furthermore, we find that the Soret coefficient, when normalized by the solute molecular volume, increases quadratically with the number of aliphatic carbons in the solvent, supporting recent studies describing the importance of dipole moments in determining the Soret effect. To our knowledge, non-methylated aromatic molecules beyond single-ringed aromatic structures and aromatic structures beyond two rings have not been presented in the literature of thermodiffusion in binary mixtures. These results may facilitate improved theoretical explanations of both the Soret effect and thermodiffusion in non-aqueous systems.

As expected, Fickian diffusion slows down as a result of increasing molecular size and solvent viscosity, with solvent viscosity dominating the dependence of D. By fixing the solvent and comparing different aromatic mixtures, we observe the secondary importance of solute molecular weight. The behavior of thermal separation, or thermal diffusion, presents a more nuanced picture. Our investigation suggests that shorter chain alkane solvents may enhance the importance of aromatic ring size in determining thermodiffusive behavior. The ring size of the solute compounds plays an important role in determining their thermophoretic behavior in alkane solutions, with larger ringed systems exhibiting greater thermal separation from alkane solvents. By increasing the size of the aromatic ringed compounds, we can begin to intuit the behavior of even larger ringer systems, ultimately approaching aromatic molecules like asphaltenes. Comparison with the literature data on methylated aromatic solvents suggests that adding even a single methyl group, for instance converting naphthalene (R2) to methylnaphthalene (mR2), can have a strong effect in reducing the thermodiffusion coefficient.

ACKNOWLEDGMENTS

The authors wish to acknowledge the member companies of the Reservoir Engineering Research Institute for funding. Jan Sengers of the University of Maryland donated both the laser light source and linear detector. The Gibbs Machine Shop and Glassblowing Service at Yale provided machining assistance for various components of the OBD cell. S.M.H thanks Don Jacobs, Glenn Weston-Murphy, Ed Jackson, Brendan Ford, and Ross Boltyanskiy for their helpful input on electronic and optical design components and J. Wambui Mutoru for coding assistance.

[1]K. Ghorayeb, A. Firoozabadi, and T. Anraku, SPE J. **8**, 114–123 (2003).
[2]K. J. Zhang, M. E. Briggs, R. W. Gammon, and J. V. Sengers, J. Chem. Phys. **104**, 6881 (1996).
[3]A. Leahy-Dios and A. Firoozabadi, J. Phys. Chem. B **111**, 191–198 (2007).
[4]A. Leahy-Dios, L. Zhou, and A. Firoozabadi, J. Phys. Chem. B **112**, 6442–6447 (2008).
[5]P. Polyakov, E. Rossinsky, and S. Wiegand, J. Phys. Chem. B **113**, 13308–13312 (2009).
[6]S. Srinivasan, D. A. de Mezquia, M. M. Bou-Ali, and M. Z. Saghir, Philos. Mag. **91**, 4332–4344 (2011).
[7]J. K. Platten, J. Appl. Mech. **73**, 5 (2006).
[8]C. Debuschewitz and W. Kohler, Phys. Rev. Lett. **87**, 055901 (2001).
[9]S. Hartmann, W. Kohler, and K. I. Morozov, Soft Matter **8**, 1355–1360 (2012).
[10]P.-A. Artola and B. Rousseau, J. Chem. Phys. **143**, 174503 (2015).
[11]V. Eric and D. A. D. Anslyn, *Modern Physical Organic Chemistry* (University Science Books, Sausalito, CA, 2006).
[12]A. J. Rodriguez, F. Capasso, and S. G. Johnson, Nat. Photonics **5**, 211 (2011).
[13]T. R. Kirkpatrick, J. M. O. de Zarate, and J. V. Sengers, Phys. Rev. Lett. **115**, 035901 (2015).
[14]G. Portella, J. Poater, and M. Sola, J. Phys. Org. Chem. **18**, 785 (2005).
[15]I. A. Popov and A. I. Boldyrev, Eur. J. Org. Chem. **2012**, 3485.
[16]A. Koniger, B. Meier, and W. Kohler, Philos. Mag. **89**, 907–923 (2009).
[17]P. Kolodner, H. Williams, and C. Moe, J. Chem. Phys. **88**, 6512 (1988).
[18]K. B. Haugen and A. Firoozabadi, J. Phys. Chem. B **110**, 17678 (2006).
[19]A. Koniger, W. Wunderlich, and W. Kohler, J. Chem. Phys. **132**, 174506 (2010).
[20]K. Lonsdale, Proc. R. Soc. A **133**, 536 (1931).
[21]R. Heyrovska, preprint arXiv:0806.4502 (2008).
[22]P. Polyakov, E. Rossinsky, and S. Wiegand, J. Phys. Chem. B **110**, 26215 (2006).
[23]H. Korsching, Z. Naturforsch. **29A** (1914).
[24]J. Demichowicz-Pigoniowa, M. Mitchell, and H. J. V. Tyrrell, J. Chem. Soc. A **1971**, 307.
[25]M. M. Bou-Ali, O. Ecenarro, J. A. Madariaga, C. M. Santamaria, and J. J. Valencia, J. Phys.: Condens. Matter **10**, 3321 (1998).